DNS of Bubble Dynamics in the Wobbling Regime using the Unstructured Conservative Level-Set Method. *

Néstor Balcázar-Arciniega[1][0000−0003−0776−2086], Joaquim Rigola[1][0000−0002−6685−3677], and Assensi Oliva[1][0000−0002−2805−4794]

[1] Heat and Mass Transfer Technological Center (CTTC), Universitat Politècnica de Catalunya-BarcelonaTech (UPC). Colom 11, 08222, Terrassa (Barcelona), Spain
nestor.balcazar@upc.edu, nestorbalcazar@yahoo.es

Abstract. Direct Numerical Simulation (DNS) of hydrodynamics and mass transfer in bubbles in the wobbling regime is reported using the Unstructured Conservative Level Set (UCLS) method. The finite-volume method on 3D collocated unstructured meshes discretizes the transport equations. The fractional-step projection method solves the pressure-velocity coupling in the momentum equation. Unstructured flux limiter schemes discretize the convective term of transport equations to minimize the numerical diffusion and avoid numerical oscillations in regions with strong gradients. The combination of these numerical schemes proves to keep the numerical stability of bubbles in the wobbling regime, that is, high Reynolds and Eötvös numbers. Numerical and physical findings on the hydrodynamics and mass transfer in wobbling bubbles are reported.

Keywords: Bubbles · Mass transfer · Unstructured Conservative Level-Set Method · Finite-Volume Method · Unstructured Meshes · Unstructured Flux-Limiters · Direct Numerical Simulation · High-Performance Computing

1 Introduction

Two-phase flow-transport processes are ubiquitous in nature and industry, significantly affecting various engineering systems, from steam generators and cooling towers in thermal power plants to various chemical engineering unit operations. Bubbles and droplets are critical in applications such as separation processes, e.g., distillation, and to improve chemical reaction processes within multiphase chemical reactors. Consequently, beyond scientific motivation, a deep understanding of the complex interactions between fluid mechanics and transport phenomena in multiphase flows is essential to designing and optimizing multiphase engineering systems effectively.

Experimental studies of multiphase flows, e.g., bubbly flows, often face limitations due to restricted optical access, while analytical approaches usually require simplifying

* The principal author, N. Balcázar-Arciniega, as a Serra-Hunter Fellow (UPC-LE8027), acknowledges the financial support provided by the Catalan Government through this program. Simulations were performed on the MareNostrum V supercomputer at the BSC, Barcelona, Spain, using computing resources allocated by the RES under grants IM-2024-2-0020 and IM-2024-3-0018. The financial support from MINECO, Spain (project PID2020-115837RB-100), is gratefully acknowledged.

ICCS Camera Ready Version 2025
To cite this paper please use the final published version:
DOI: 10.1007/978-3-031-97570-7_29

assumptions that may not capture all essential physics. With advances in supercomputing, Direct Numerical Simulation (DNS) [42,53] has emerged as a powerful alternative to overcome these challenges, particularly in investigating the complex dynamics of bubbles in the wobbling regime.

Various interface-capturing techniques have been developed to simulate multiphase flows accurately. These include front-tracking (FT) methods [55,51], level-set (LS) approaches [40,48,28], conservative level-set (CLS) methods [39,11,7,14,17], Volume of Fluid (VoF) techniques [31], and hybrid VoF-LS strategies [47,46,6]. Moreover, some of them have been extended to address complex phenomena such as mass and heat transfer in single bubbles [23,18,22] and bubble swarms [1,45,35,14,17], variable surface tension in two-phase flows [13,8], and liquid-vapor phase change [57,29,54,32,15].

According to the Grace diagram for bubbles that rise under gravity [21], when viscous and/or surface tension forces dominate over inertial forces, bubbles tend to remain nearly spherical. As the viscosity of the fluid around the bubble and surface tension coefficient decrease, bubbles transition into the ellipsoidal regime, where they become oblate with a convex interface across their entire surface and frequently exhibit periodic dilations or random wobbling motions. In this context, bubbles with surface oscillations and path instabilities, hereafter referred to as the wobbling regime, occur at high Reynolds numbers and intermediate Eötvös numbers, which is the range of dimensionless parameters focused on in this research.

DNS of bubbles with interfacial transport processes in the wobbling regime presents several numerical challenges. These include issues such as numerical diffusion [41], oscillations near discontinuities, high computational costs associated with large density ratios, numerical coalescence, and accurate calculation of surface tension forces. In this work, these challenges are effectively addressed using the Unstructured Conservative Level Set (UCLS) method introduced and further extended by Balcazar et al. [11,14,7,17], which has been tailored to capture the intricate dynamics of wobbling bubbles with interfacial heat and mass transfer.

The UCLS method [11,12,7,13,14,17] incorporates several key innovations. It employs an optimized interface thickness through careful tuning of the conservative level-set parameters and uses a least-squares approach to compute accurate interface normals, which are essential for precise surface tension force calculations. Moreover, by smoothing the physical properties across the interface, the UCLS method mitigates numerical instabilities. On the other hand, the multiple marker strategy [7,14,17] is implemented to avoid the so-called numerical coalescence. The appropriate selection of unstructured flux limiter convection schemes, proposed by [11] in the framework of the UCLS method, minimizes numerical diffusion and suppresses oscillations across discontinuities. Although these schemes have been successfully applied to bubbly flows [17], their impact on the simulation of mass transfer and hydrodynamics of two bubbles in a vertical pipe remains an area for further exploration. This work contributes to bridging that gap while advancing numerical models for multiphase transport processes within the UCLS framework.

The remainder of the paper is organized as follows. Section 2 details the mathematical formulation and numerical methods employed. Section 3 presents numerical experiments that examine the dynamics of gravity-driven bubbles in the wobbling regime.

ICCS Camera Ready Version 2025
To cite this paper please use the final published version:
DOI: 10.1007/978-3-031-97570-7_29

Finally, Section 4 summarizes the conclusions and outlines the directions for future research.

2 Mathematical Formulation and Numerical Methods

2.1 Transport Equations

The governing Navier-Stokes equations for both the dispersed phase (Ω_d) and the continuous phase (Ω_c) are solved within the framework of the one-fluid formulation [52,43], adapted to the multi-marker UCLS approach [14,7,17]:

$$\frac{\partial}{\partial t}(\rho \mathbf{v}) + \nabla \cdot (\rho \mathbf{v}\mathbf{v}) = -\nabla p + \nabla \cdot \mu \left(\nabla \mathbf{v}\right) + \nabla \cdot \mu (\nabla \mathbf{v})^T + (\rho - \rho_0)\mathbf{g} + \mathbf{f}_\sigma, \quad (1)$$

$$\nabla \cdot \mathbf{v} = 0, \quad (2)$$

where p is the pressure, $\mathbf{v}$ denotes the fluid velocity, μ is the viscosity, ρ is the fluid density, $\mathbf{g}$ refers to the gravitational acceleration, $\mathbf{f}_\sigma$ is the surface tension force per unit volume concentrated on the interface. Subscripts d and c refer to the dispersed and continuous phases, respectively. Within each phase, the density and viscosity are constant, but they exhibit a discontinuity at the interface: $\rho = \rho_c H_c + \rho_d H_d$, $\mu = \mu_c H_c + \mu_d H_d$, where H_c is the Heaviside step function (equal one in Ω_c and zero elsewhere), and $H_d = 1 - H_c$. When periodic boundary conditions are applied along the y-axis (aligned with $\mathbf{g}$), the average density is $\rho_0 = V_\Omega^{-1} \int_\Omega (\rho_c H_c + \rho_d H_d)\, dV$, as included in Eq.(1) [14,3,7,17]. Otherwise ρ_0 is set to zero.

Interface capturing is solved by the Unstructured Conservative Level-Set (UCLS) method proposed by Balcazar et al. [14,11,12,17] on three-dimensional collocated unstructured meshes and implemented by the finite-volume method. To prevent the numerical coalescence of fluid particles, the multi-marker UCLS approach is utilized [14,7,3,17]. In this framework, a regularized signed distance function is assigned to each marker, $\phi_i = \frac{1}{2}\left(\tanh\left(\frac{d_i}{2\varepsilon}\right) + 1\right)$, where d_i is a signed distance function [40,49], and ε determines the thickness of the interface profile [14,7,3,17]. The UCLS advection equation is solved in conservative form for each marker:

$$\frac{\partial \phi_i}{\partial t} + \nabla \cdot (\phi_i \mathbf{v}) = 0, \;\; i = \{1, 2, ..., N_m - 1, N_m\}. \quad (3)$$

with N_m representing the total number of markers (which corresponds to the number of fluid particles). To maintain the level-set profile, the following unstructured reinitialization equation [11,12,14,17] is solved:

$$\frac{\partial \phi_i}{\partial \tau} + \nabla \cdot \left(\phi_i(1-\phi_i)\mathbf{n}_i^0\right) = \nabla \cdot \left(\varepsilon \nabla \phi_i\right), \;\; i = \{1, 2, ..., N_m - 1, N_m\}, \quad (4)$$

where the equation is evolved in pseudo-time τ until the steady state is reached. Here, $\mathbf{n}_i^0$ is the unit normal vector at the interface evaluated at $\tau = 0$. At the control volume Ω_P, $\varepsilon_P = 0.5(h_P)^\alpha$, $\alpha = [0.9, 1]$ (unless otherwise stated) and h_P is the characteristic local

ICCS Camera Ready Version 2025
To cite this paper please use the final published version:
DOI: 10.1007/978-3-031-97570-7_29

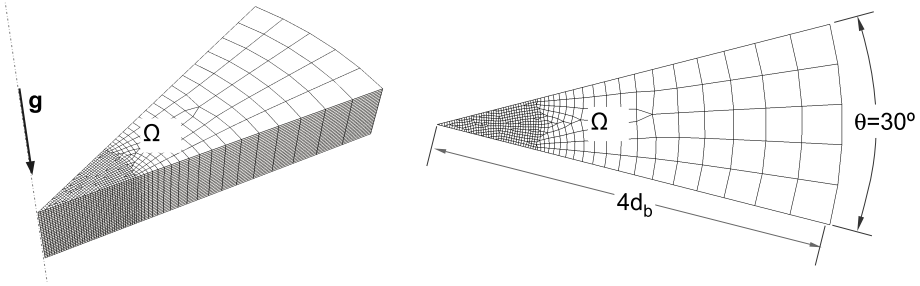

Fig. 1. Scheme for mesh distribution for axial-symmetric cases. Control volumes combines hexahedrals and triangular prisms. Ω is a section of a cylindrical domain, with $\theta = 30^{\circ}$, $R = 4\,d_b$ and $L_y = 12\,d_b$ (parallel to $\mathbf{g}$). Here, d_b is the spherical equivalent bubble diameter.

grid size [11,12,14,17]. Interface normal vectors ($\mathbf{n}_i$) and curvatures (κ_i) are computed by $\mathbf{n}_i = \nabla\phi_i \; ||\nabla\phi_i||^{-1}$, $\kappa_i = -\nabla \cdot \mathbf{n}_i$ [11,12,14,17].

The surface tension force, $\mathbf{f}_\sigma$ (see Eq.(1)), is computed using the Continuous Surface Force (CSF) model [19], extended for the multi-marker UCLS framework as proposed by Balcazar et al. [7,13,3,14,17]:

$$\mathbf{f}_\sigma = \sum_{i=1}^{N_m} (\mathbf{f}_{\sigma,i}^{(n)} + \mathbf{f}_{\sigma,i}^{(t)}). \tag{5}$$

In this formulation, the tangential component, $\mathbf{f}_{\sigma,i}^{(t)}$, represents the Marangoni force [24] and is defined as $\mathbf{f}_{\sigma,i}^{(t)} = \delta_{\Gamma,i}^{s} \nabla_{\Gamma_i}\sigma$ [7,13,3,14,17], σ is the surface tension coefficient. In the present study, σ is constant, and hence $\mathbf{f}_{\sigma,i}^{(t)} = \mathbf{0}$. On the other hand, the normal component of the surface tension force, perpendicular to the interface (Γ_i), is calculated as $\mathbf{f}_{\sigma,i}^{(n)} = \sigma\kappa_i\nabla\phi_i$ [11,12,13,3,14,17].

For external mass transfer [21], the concentration (C) of a chemical species evolves according to

$$\frac{\partial C}{\partial t} + \nabla \cdot (\mathbf{v}C) = \nabla \cdot (\mathcal{D}\nabla C), \tag{6}$$

which is solved in the continuous phase, Ω_c. Here, $\mathcal{D} = \mathcal{D}_c$ is the diffusivity. The concentration inside the bubbles remains constant, while the concentration in the interface cells is calculated using the unstructured interpolation method proposed by Balcazar-Arciniega et al. [14].

2.2 Numerical methods

Transport equations are discretized using the finite-volume method on three-dimensional collocated unstructured meshes [14,17]. In this framework, convective terms are discretized using unstructured flux limiter schemes proposed by Balcazar et al. [11,14,16,17]. Specifically, for a control volume Ω_P the convective term is written as $(\nabla \cdot \beta\psi\mathbf{v})_P =$

ICCS Camera Ready Version 2025
To cite this paper please use the final published version:
DOI: 10.1007/978-3-031-97570-7_29

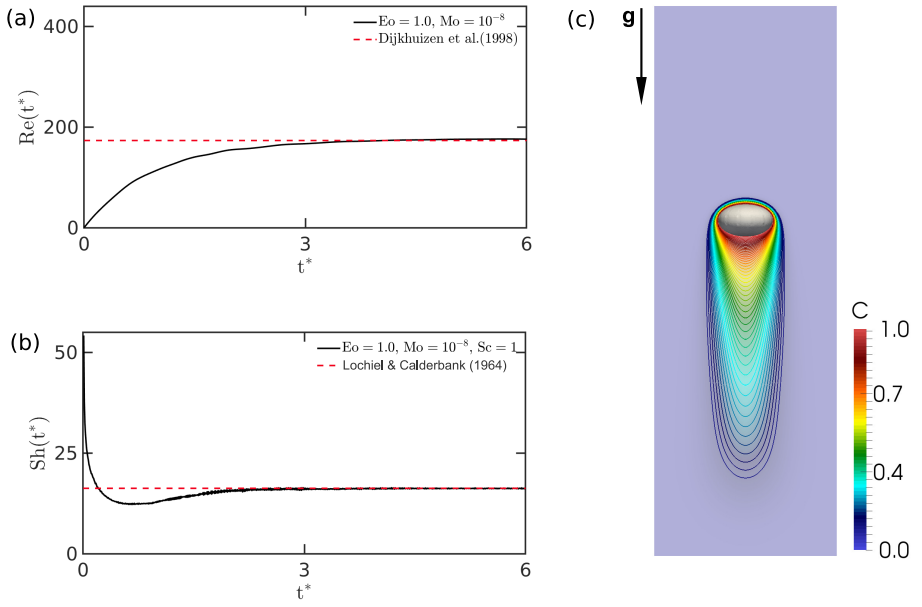

Fig. 2. Axial-symmetric rising bubble. Eo $= 1.0$, Mo $= 10^{-8}$, Sc $= 1$, $\eta_\rho = \eta_\mu = 100$. (a) Reynolds number, UCLS method versus correlation from Dijkhuizen et al. [25]. (b) Sherwood number, UCLS method versus correlation from Lochiel and Calderbank [38]. (c) Concentration of a chemical species at $t^* = 6.3$.

$V_P^{-1} \sum_f \beta_f \psi_f (\mathbf{v}_f \cdot \mathbf{A}_f)$, where $\mathbf{A}_f = A_f \, \mathbf{e}_f$ denotes the area vector at face f, V_P denotes the volume of Ω_P, and $\mathbf{e}_f$ is a unit-vector pointing outside Ω_P. Moreover,

$$\psi_f = \psi_{C_p} + \frac{1}{2}\mathbf{L}(\theta_f)(\psi_{D_p} - \psi_{C_p}), \tag{7}$$

with the monitor variable $\theta_f = (\psi_{C_p} - \psi_{U_p})/(\psi_{D_p} - \psi_{C_p})$, and $L(\theta_f)$ representing the flux limiter function. In this notation, the subindex D_p designates the downwind point, subindex C_p is the upwind point, subindex U_p is the far-upwind point, following the stencil outlined for both single and multi-marker UCLS methods [11,14,17]. Some of the flux-limiter functions [50,27,30,36,34] implemented in the framework of the UCLS method [16,17] are given by:

$$L(\theta_f) \equiv \begin{cases} \max\{0, \min\{2\theta_f, 1\}, \min\{2, \theta_f\}\} & \text{SUPERBEE}, \\ \max\{0, \min\{2\theta_f, (2/3)\,\theta_f + (1/3), 2\}\} & \text{KOREN}, \\ \max\{0, \min\{4\theta_f, 0.75 + 0.25\theta_f, 2\}\} & \text{SMART}, \\ (\theta_f + |\theta_f|)/(1 + |\theta_f|) & \text{VANLEER}, \\ \text{minmod}\{1, \theta_f\} & \text{MINMOD}, \\ 0 & \text{UPWIND}, \\ 1 & \text{CD}. \end{cases} \tag{8}$$

ICCS Camera Ready Version 2025
To cite this paper please use the final published version:
DOI: 10.1007/978-3-031-97570-7_29

Hereafter, the Total Variation Diminishing (TVD) [37] SUPERBEE flux-limiter function is selected, unless otherwise stated. The diffusive term of the transport equations is discretized with a central difference scheme [14,17]. Gradients are evaluated using the weighted least-squares method unless otherwise stated [9,11,14]. The pressure-velocity coupling is solved with the fractional-step projection method [20,43,52]:

$$\frac{\rho_P \mathbf{v}_P^* - \rho_P^0 \mathbf{v}_P^0}{\Delta t} = \mathbf{C}_{\mathbf{v},P}^0 + \mathbf{D}_{\mathbf{v},P}^0 + (\rho_P - \rho_0)\mathbf{g} + \mathbf{f}_{\sigma,P}, \tag{9}$$

$$\left(\nabla \cdot \left(\frac{\Delta t}{\rho}\nabla p\right)\right)_P = (\nabla \cdot \mathbf{v}^*)_P\,,\ \mathbf{e}_{\partial\Omega} \cdot \nabla p|_{\partial\Omega} = 0. \tag{10}$$

$$\frac{\rho_P \mathbf{v}_P - \rho_P \mathbf{v}_P^*}{\Delta t} = -(\nabla p)_P. \tag{11}$$

Here, the superscript 0 refers to the previous time step. Furthermore, $\mathbf{D}_\mathbf{v} = \nabla \cdot \mu \nabla \mathbf{v} + \nabla \cdot \mu (\nabla \mathbf{v})^T$, $\mathbf{C}_\mathbf{v} = -\nabla \cdot (\rho \mathbf{v}\mathbf{v})$, $\mathbf{v}_P^*$ is the predictor velocity, and $\mathbf{v}_P$ is the corrected velocity. The linear system that arises from Eq. (10) is solved by the preconditioned conjugate gradient method (Jacobi preconditioner) [33,56]. The boundary $\partial\Omega$ excludes regions with periodic conditions, where information from the corresponding periodic nodes is used [14,12,7]. Finally, a convective velocity ($\mathbf{v}_f$) [11,12,14,13,17] is interpolated on the faces of the cell to avoid the decoupling of pressure-velocity in the framework of collocated meshes [44]. This convective velocity leads to the volume flux ($\mathbf{v}_f \cdot \mathbf{A}_f$), which is used in the discretized convective term. The reader is referred to Balcazar-Arciniega et al. [14,17] for further technical details on finite-volume discretizations.

3 Numerical Experiments

Multiple verifications, validations, and extensions of the Unstructured Conservative Level-Set (UCLS) method have been reported, including single rising bubbles [11,12,3], falling droplets [5], bubble swarms [7,3,14,9,17], binary droplet collision [7], collision of a droplet against an interface [7], deformation of droplets under shear stresses [6], mass transfer in bubbly flows [10,2,14,9,17], variable surface tension [13], and liquid-vapor phase change [4,15]. Consequently, this research represents a further step in the simulation of bubbly lows with interfacial mass transfer within the framework of the UCLS method [11,14,7,15,17].

Gravity-driven rising bubbles are characterized by the Morton number $\mathrm{Mo} = g\mu_c^4(\rho_c - \rho_d)\rho_c^{-2}\sigma^{-3}$, Eötvös number $\mathrm{Eo} = g d_b^2(\rho_c - \rho_d)\sigma^{-1}$, density ratio $\eta_\rho = \rho_c/\rho_d$, viscosity ratio $\eta_\mu = \mu_c/\mu_d$, and Reynolds number $\mathrm{Re_i(t^*)} = \rho_c \mathrm{U_{r,i}} d_b/\mu_c$, $\mathrm{Re(t^*)} = N_b^{-1}\sum_{i=1}^{N_b}\mathrm{Re_i(t^*)}$, $\mathrm{Re_i} = T^{-1}\int_{t_0}^{t_0+T}\mathrm{Re_i(t)}dt$, $\mathrm{Re} = N_b^{-1}\sum_{i=1}^{N_b}\mathrm{Re_i}$. Here, d_b refers to the equivalent diameter of the initial spherical bubble, $V_{\Omega_{d,d}}$ is the volume of bubbles, $\mathrm{U_{r,i}}$ is the velocity of the bubble with respect to the velocity of the continuous phase, the subindex i refers to the i-th bubble, and $\mathrm{t^*} = t\, g^{1/2}\, d_b^{-1/2}$. Furthermore, mass transfer is characterized by the Schmidt number $\mathrm{Sc} = \mu_c/(\rho_c \mathcal{D}_c)$ and the Sherwood number $\mathrm{Sh} = k_c d_b/\mathcal{D}_c$. Here, k_c denotes the mass transfer coefficient at Ω_c [14,17].

ICCS Camera Ready Version 2025
To cite this paper please use the final published version:
DOI: 10.1007/978-3-031-97570-7_29

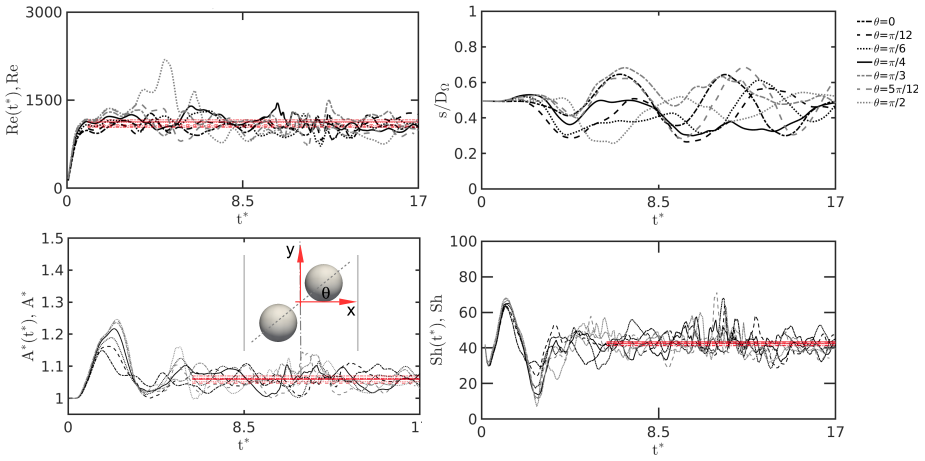

Fig. 3. Two bubbles rising in a vertical pipe. Effect of the initial configuration angle (θ). Eo $= 3.125$, Mo $= 10^{-11}$, Sc $= 1$, $\eta_\rho = \eta_\mu = 100$, Da $= 0$, $\mathrm{C_R} = \mathrm{d_b/D_\Omega} = 0.33$. Reynolds number Re, dimensionless centroid-centroid distance $\mathrm{s\,D_\Omega^{-1}}$, normalized interfacial area $\mathrm{A^*} = \mathrm{A}\,(N_b\,4\,\pi r_b^2)^{-1}$, $\mathrm{A} = \sum_{i=1}^{N_b} A_i$, $A_i = \int_\Omega \delta^s_{\Gamma,i}\,dV$, $\delta^s_{\Gamma,i} = ||\nabla\phi_i||$ [11,14,17].

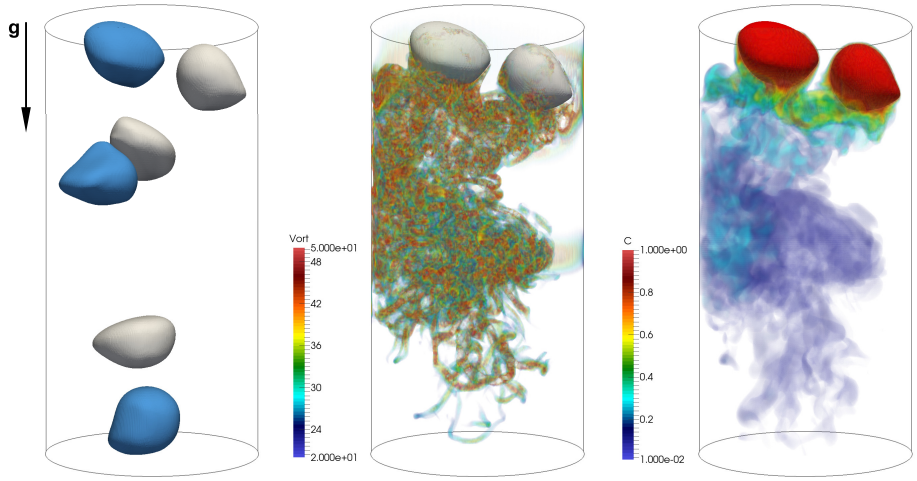

Fig. 4. Two bubbles rising in a vertical pipe. Eo $= 3.125$, Mo $= 10^{-11}$, Sc $= 1$, $\eta_\rho = \eta_\mu = 100$, Da $= 0$, $\mathrm{C_R} = \mathrm{d_b/D_\Omega} = 0.33$, $\theta = (1/2), \pi$. Bubble interaction at $t^* = \{1.2,\ 1.9,\ 2.2\}$. Vorticity norm, $||\nabla \times \mathbf{v}||$, at $t^* = 2.2$. Normalized concentration of the chemical species, C, at $t^* = 2.2$.

Figure 1 depicts the computational setup for single bubbles within an axially symmetric domain. Ω is discretized by 277 440 hexahedral and triangular prism control

ICCS Camera Ready Version 2025
To cite this paper please use the final published version:
DOI: 10.1007/978-3-031-97570-7_29

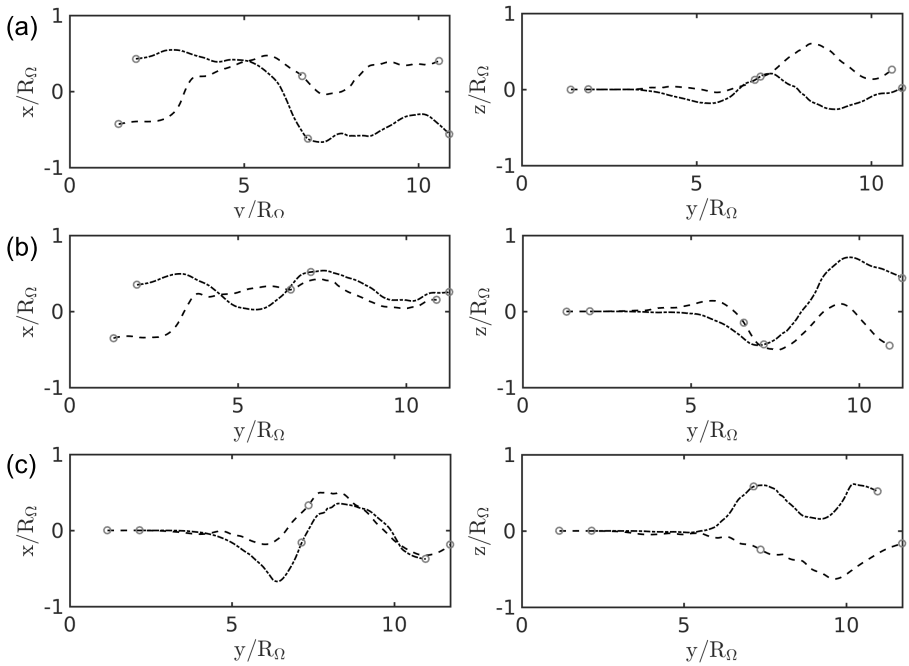

Fig. 5. Trajectories of two bubbles rising in a vertical pipe. Effect of the initial configuration angle (θ). Eo $= 3.125$, Mo $= 10^{-11}$, Sc $= 1$, $\eta_\rho = \eta_\mu = 100$, Da $= 0$, $\mathrm{C_R} = \mathrm{d_b/D_\Omega} = 0.33$. (a) $\theta = (1/6)\,\pi$. (b) $\theta = (1/4)\,\pi$. (c) $\theta = (1/2)\,\pi$.

volumes, distributed 14 CPU-cores. The minimum grid resolution is $h_{\min} = d_b/40$ around the symmetry axis, which is enough to solve the hydrodynamics and mass transfer (Sc $= 1$) in bubbles [14,17]. The nonslip boundary condition is applied to the upper and lower boundaries, and the Neumann condition is applied to the lateral walls. The Neumann boundary conditions are used for $\{\phi, C\}$. Initially, the bubble is set on the symmetry axis, at $2\,d_b$ from the bottom. The fluids are initially at rest.

Figure 2 shows the UCLS simulation of the rising bubble in the axially symmetric domain, with dimensionless numbers Eo $= 1.0$, Mo $= 10^{-8}$, Sc $= 1$, $\eta_\rho = \eta_\mu = 100$, Da $= 0$. With respect to the Reynolds number, the results of the UCLS simulation closely match those obtained using the correlation of the drag coefficient proposed in [25]. Moreover, the Sherwood number calculated using the UCLS method shows excellent agreement with the correlation reported by Lochiel and Calderbank [38]. Figure 2 also shows a snapshot of the concentration of chemical species in $t^* = 6.3$.

In a further step, the dynamics of two bubbles rising in a vertical pipe is researched. The domain consists of a vertical pipe with radius $R_\Omega = 3\,d_b$ ($D_\Omega = 2\,R_\Omega$) and height $H_\Omega = 12\,d_b$. Ω is discretized by 12.16×10^6 triangular prisms, distributed on 384 CPU cores. The mesh has the maximum grid size $h_{max} \approx d_b/35$ around the center of the channel, refined to $h_{min} = h_{max}/3$ close to the wall. The initial configuration of the

ICCS Camera Ready Version 2025
To cite this paper please use the final published version:
DOI: 10.1007/978-3-031-97570-7_29

two bubbles is shown in Figure 3. Here, θ is the configuration angle at $t^* = 0$. Furthermore, s/D_Ω denotes the normalized distance between the bubble centroids, which is set to $s/D_\Omega = 0.5$ at $t^* = 0$. Figure 3 depicts $\mathrm{Re(t^*)}$, $\mathrm{Sh(t^*)}$, normalized interfacial area $\mathrm{A^*} = \mathrm{A}\,(N_b\,4\,\pi r_b^2)^{-1}$, $\mathrm{A} = \sum_{i=1}^{N_b} A_i$, $A_i = \int_\Omega \delta^s_{\Gamma,i}\,dV$, $\delta^s_{\Gamma,i} = ||\nabla\phi_i||$, [11,14,17], and normalized distance s/D_Ω between bubble centroids. The Reynolds number averaged over time is in the range $[1037.3,\ 1164.2]$, while the Sherwood number is in the range $[41.2,\ 43.5]$. Figure 4 shows a set of snapshots for bubble-bubble and bubble-wall interactions, as well as the vorticity norm and concentration at $t^* = 2.2$. Figure 5 shows the effect of the initial configuration angle on the trajectories of the two bubbles rising in the vertical pipe for $\theta = \{(1/6)\,\pi,\ (1/4)\,\pi\,,(1/2)\,\pi\}$.

4 Conclusions

The numerical results demonstrated the precision and numerical robustness of the multiple-marker UCLS method proposed by Balcazar et al. [11,12,14,13,17] to simulate the hydrodynamics and mass transfer of two wobbling bubbles that rise in a vertical pipe. In the context of single-bubble simulations, the results for the predicted Reynolds number and Sherwood number are in excellent agreement with the correlations in the literature [25,38]. Concerning the dynamics of two bubbles, UCLS simulations demonstrate the drafting-kissing-tumbling mechanism [26] for bubble-bubble interaction and a repulsion effect for bubble-wall interaction. Furthermore, Re and Sh have a very small sensitivity to θ. Our future efforts will focus on applying and extending the multiple-marker UCLS method to simulate bubbly flows with variable surface tension, liquid-vapor phase change, and simultaneous heat and mass transfer.

References

1. Aboulhasanzadeh, B., Thomas, S., Taeibi-Rahni, M., Tryggvason, G.: Multiscale computations of mass transfer from buoyant bubbles. Chemical Engineering Science **75**, 456–467 (6 2012). https://doi.org/10.1016/j.ces.2012.04.005, https://linkinghub.elsevier.com/retrieve/pii/S000925091200231X
2. Balcazar, N., Antepara, O., Rigola, J., Oliva, A.: Dns of drag-force and reactive mass transfer in gravity-driven bubbly flows. In: García-Villalba, M., Kuerten, H., Salvetti, M. (eds) Direct and Large Eddy Simulation XII. DLES 2019. ERCOFTAC Series, vol 27. Springer, Cham pp. 119–125 (2020). https://doi.org/10.1007/978-3-030-42822-8$_1$6, http://link.springer.com/10.1007/978-3-030-42822-8_16
3. Balcazar, N., Castro, J., Rigola, J., Oliva, A.: Dns of the wall effect on the motion of bubble swarms. Procedia Computer Science **108**, 2008–2017 (2017). https://doi.org/10.1016/j.procs.2017.05.076, https://linkinghub.elsevier.com/retrieve/pii/S1877050917306142
4. Balcazar, N., Rigola, J., Oliva, A.: Unstructured level-set method for saturated liquid-vapor phase change. In: WCCM-ECCOMAS 2020. Volume 600 - Fluid Dynamics and Transport Phenomena. pp. 1–12 (2021). https://doi.org/10.23967/wccm-eccomas.2020.352, https://www.scipedia.com/public/Balcazar_et_al_2021a
5. Balcazar, N., Castro, J., Chiva, J., Oliva, A.: Dns of falling droplets in a vertical channel. International Journal of Computational Methods and Experimental Measurements **6**, 398–410

ICCS Camera Ready Version 2025
To cite this paper please use the final published version:
DOI: 10.1007/978-3-031-97570-7_29

(11 2017). https://doi.org/10.2495/CMEM-V6-N2-398-410, http://www.witpress.com/doi/journals/CMEM-V6-N2-398-410
6. Balcazar, N., Lehmkuhl, O., Jofre, L., Rigola, J., Oliva, A.: A coupled volume-of-fluid/level-set method for simulation of two-phase flows on unstructured meshes. Computers and Fluids **124**, 12–29 (2016). https://doi.org/10.1016/j.compfluid.2015.10.005, https://linkinghub.elsevier.com/retrieve/pii/S0045793015003394
7. Balcazar, N., Lehmkuhl, O., Rigola, J., Oliva, A.: A multiple marker level-set method for simulation of deformable fluid particles. International Journal of Multiphase Flow **74**, 125–142 (2015). https://doi.org/10.1016/j.ijmultiphaseflow.2015.04.009
8. Balcazar-Arciniega, N., Rigola, J., Oliva, A.: A level-set model for two-phase flow with variable surface tension: Thermocapillary and surfactants. 8th European Congress on Computational Methods in Applied Sciences and Engineering (2022). https://doi.org/10.23967/eccomas.2022.011, https://www.scipedia.com/public/Balcazar_Arciniega_et_al_2022a
9. Balcazar-Arciniega, N., Rigola, J., Oliva, A.: Dns of mass transfer from bubbles rising in a vertical channel. Lecture Notes in Computer Science (including subseries Lecture Notes in Artificial Intelligence and Lecture Notes in Bioinformatics) **11539 LNCS**, 596–610 (2019). https://doi.org/10.1007/978-3-030-22747-0_45, http://link.springer.com/10.1007/978-3-030-22747-0_45
10. Balcazar-Arciniega, N., Rigola, J., Oliva, A.: Dns of mass transfer in bi-dispersed bubble swarms. In: Computational Science – ICCS 2022. ICCS 2022. Lecture Notes in Computer Science, vol 13353. Springer, Cham **13353**, 284–296 (2022). https://doi.org/10.1007/978-3-031-08760-8_24, https://link.springer.com/10.1007/978-3-031-08760-8_24
11. Balcázar, N., Jofre, L., Lehmkuhl, O., Castro, J., Rigola, J.: A finite-volume/level-set method for simulating two-phase flows on unstructured grids. International Journal of Multiphase Flow **64**, 55–72 (2014). https://doi.org/10.1016/j.ijmultiphaseflow.2014.04.008
12. Balcázar, N., Lehmkuhl, O., Jofre, L., Oliva, A.: Level-set simulations of buoyancy-driven motion of single and multiple bubbles. International Journal of Heat and Fluid Flow **56**, 91–107 (12 2015). https://doi.org/10.1016/j.ijheatfluidflow.2015.07.004
13. Balcázar, N., Rigola, J., Castro, J., Oliva, A.: A level-set model for thermocapillary motion of deformable fluid particles. International Journal of Heat and Fluid Flow **62**, 324–343 (12 2016). https://doi.org/10.1016/j.ijheatfluidflow.2016.09.015, https://linkinghub.elsevier.com/retrieve/pii/S0142727X16301266
14. Balcázar-Arciniega, N., Antepara, O., Rigola, J., Oliva, A.: A level-set model for mass transfer in bubbly flows. International Journal of Heat and Mass Transfer **138**, 335–356 (8 2019). https://doi.org/10.1016/j.ijheatmasstransfer.2019.04.008
15. Balcázar-Arciniega, N., Rigola, J., Oliva, A.: Unstructured Conservative Level-Set (UCLS) Simulations of Film Boiling Heat Transfer, pp. 318–331 (2023). https://doi.org/10.1007/978-3-031-36030-5_26, https://link.springer.com/10.1007/978-3-031-36030-5_26
16. Balcázar-Arciniega, N., Rigola, J., Oliva, A.: Unstructured flux-limiter convective schemes for simulation of transport phenomena in two-phase flows. In: Lecture Notes in Computer Science (including subseries Lecture Notes in Artificial Intelligence and Lecture Notes in Bioinformatics). vol. 14838 LNCS, pp. 20–32. Springer Science and Business Media Deutschland GmbH (2024). https://doi.org/10.1007/978-3-031-63783-4_3
17. Balcázar-Arciniega, N., Rigola, J., Pérez-Segarra, C.D., Oliva, A.: Numerical study of the drag force, interfacial area and mass transfer in bubbles in a vertical pipe. Chemical Engineering Journal **495**, 153124 (9 2024). https://doi.org/10.1016/j.cej.2024.153124, https://linkinghub.elsevier.com/retrieve/pii/S1385894724046126

ICCS Camera Ready Version 2025
To cite this paper please use the final published version:
DOI: 10.1007/978-3-031-97570-7_29

18. Bothe, D., Fleckenstein, S.: A volume-of-fluid-based method for mass transfer processes at fluid particles. Chemical Engineering Science (2013). https://doi.org/10.1016/j.ces.2013.05.029
19. Brackbill, J.U., Kothe, D.B., Zemach, C.: A continuum method for modeling surface tension. Journal of Computational Physics **100**, 335–354 (1992). https://doi.org/10.1016/0021-9991(92)90240-Y, https://linkinghub.elsevier.com/retrieve/pii/002199919290240Y
20. Chorin, A.J.: Numerical solution of the navier-stokes equations. Mathematics of Computation **22**, 745 (1968). https://doi.org/10.2307/2004575, https://www.jstor.org/stable/2004575?origin=crossref
21. Clift, R., Grace, J., Weber, M.: Bubbles, Drops, and Particles. DOVER PUBLICATIONS, INC (1978)
22. Darmana, D., Deen, N.G., Kuipers, J.A.M.: Detailed 3d modeling of mass transfer processes in two-phase flows with dynamic interfaces. Chemical Engineering Technology **29**, 1027–1033 (9 2006). https://doi.org/10.1002/ceat.200600156, https://onlinelibrary.wiley.com/doi/10.1002/ceat.200600156
23. Davidson, M.R., Rudman, M.: Volume-of-fluid calculation of heat or mass transfer across deforming interfaces in two-fluid flow. Numerical Heat Transfer, Part B: Fundamentals **41**, 291–308 (3 2002). https://doi.org/10.1080/104077902753541023, http://www.tandfonline.com/doi/abs/10.1080/104077902753541023
24. Deen, W.: Analysis of Transport Phenomena. OXFORD UNIV PR (2011)
25. Dijkhuizen, W., Roghair, I., Annaland, M.V.S., Kuipers, J.: Dns of gas bubbles behaviour using an improved 3d front tracking model—model development. Chemical Engineering Science **65**, 1427–1437 (2 2010). https://doi.org/10.1016/j.ces.2009.10.022, https://linkinghub.elsevier.com/retrieve/pii/S0009250909007374
26. Fortes, A.F., Joseph, D.D., Lundgren, T.S.: Nonlinear mechanics of fluidization of beds of spherical particles. Journal of Fluid Mechanics **177**, 467–483 (4 1987). https://doi.org/10.1017/S0022112087001046, https://www.cambridge.org/core/product/identifier/S0022112087001046/type/journal_article
27. Gaskell, P.H., Lau, A.K.C.: Curvature-compensated convective transport: Smart, a new boundedness- preserving transport algorithm. International Journal for Numerical Methods in Fluids **8**, 617–641 (1988). https://doi.org/10.1002/fld.1650080602, http://doi.wiley.com/10.1002/fld.1650080602
28. Gibou, F., Fedkiw, R., Osher, S.: A review of level-set methods and some recent applications. Journal of Computational Physics **353**, 82–109 (1 2018). https://doi.org/10.1016/j.jcp.2017.10.006, https://linkinghub.elsevier.com/retrieve/pii/S0021999117307441
29. Gibou, F., Chen, L., Nguyen, D., Banerjee, S.: A level set based sharp interface method for the multiphase incompressible navier–stokes equations with phase change. Journal of Computational Physics **222**, 536–555 (3 2007). https://doi.org/10.1016/j.jcp.2006.07.035, https://linkinghub.elsevier.com/retrieve/pii/S0021999106003652
30. Guenther, C., Syamlal, M.: The effect of numerical diffusion on simulation of isolated bubbles in a gas-solid fluidized bed. Powder Technology (2001). https://doi.org/10.1016/S0032-5910(00)00386-7
31. Hirt, C., Nichols, B.: Volume of fluid (vof) method for the dynamics of free boundaries. Journal of Computational Physics **39**, 201–225 (1 1981). https://doi.org/10.1016/0021-9991(81)90145-5, https://linkinghub.elsevier.com/retrieve/pii/0021999181901455

ICCS Camera Ready Version 2025
To cite this paper please use the final published version:
DOI: 10.1007/978-3-031-97570-7_29

32. Juric, D., Tryggvason, G.: Computations of boiling flows. International Journal of Multiphase Flow **24**, 387–410 (4 1998). https://doi.org/10.1016/S0301-9322(97)00050-5, https://linkinghub.elsevier.com/retrieve/pii/S0301932297000505
33. Karniadakis, G.E., II, R.M.K.: Parallel Scientific Computing in C++ and MPI. Cambridge University Press (6 2003). https://doi.org/10.1017/CBO9780511812583, https://www.cambridge.org/core/product/identifier/9780511812583/type/book
34. Koren, B.: A robust upwind discretization method for advection, diffusion and source terms. In: Numerical Methods for Advection-Diffusion Problems, C. Vreugdenhil and B. Koren, eds., vol. 45 of Notes on Numerical Fluid Mechanics, Vieweg, Braunschweig pp. 117–138 (1993)
35. Koynov, A., Khinast, J.G., Tryggvason, G.: Mass transfer and chemical reactions in bubble swarms with dynamic interfaces. AIChE Journal **51**, 2786–2800 (10 2005). https://doi.org/10.1002/aic.10529, https://onlinelibrary.wiley.com/doi/10.1002/aic.10529
36. LeVeque, R.J.: Finite Volume Methods for Hyperbolic Problems (2002). https://doi.org/10.1017/cbo9780511791253
37. LeVeque, R.J.: Finite Volume Methods for Hyperbolic Problems. Cambridge University Press (8 2002). https://doi.org/10.1017/CBO9780511791253, https://www.cambridge.org/core/product/identifier/9780511791253/type/book
38. Lochiel, A., Calderbank, P.: Mass transfer in the continuous phase around axisymmetric bodies of revolution. Chemical Engineering Science **19**, 471–484 (7 1964). https://doi.org/10.1016/0009-2509(64)85074-0
39. Olsson, E., Kreiss, G.: A conservative level set method for two phase flow. Journal of Computational Physics **210**, 225–246 (11 2005). https://doi.org/10.1016/j.jcp.2005.04.007, https://linkinghub.elsevier.com/retrieve/pii/S0021999105002184
40. Osher, S., Sethian, J.A.: Fronts propagating with curvature-dependent speed: Algorithms based on hamilton-jacobi formulations. Journal of Computational Physics **79**, 12–49 (11 1988). https://doi.org/10.1016/0021-9991(88)90002-2, https://linkinghub.elsevier.com/retrieve/pii/0021999188900022
41. Patankar, S.V.: Numerical Heat Transfer and Fluid Flow. Taylor & Francis (1980)
42. Prosperetti, A., Tryggvason, G.: Computational Methods for Multiphase Flow. Cambridge University Press (2007). https://doi.org/10.1017/CBO9780511607486
43. Prosperetti, A., Tryggvason, G.: Computational Methods for Multiphase Flow. Cambridge University Press (2007). https://doi.org/10.1017/CBO9780511607486
44. Rhie, C.M., Chow, W.L.: Numerical study of the turbulent flow past an airfoil with trailing edge separation. AIAA Journal **21**, 1525–1532 (1983). https://doi.org/10.2514/3.8284, https://arc.aiaa.org/doi/10.2514/3.8284
45. Roghair, I., Annaland, M.V.S., Kuipers, J.: An improved front-tracking technique for the simulation of mass transfer in dense bubbly flows. Chemical Engineering Science **152**, 351–369 (10 2016). https://doi.org/10.1016/j.ces.2016.06.026, https://linkinghub.elsevier.com/retrieve/pii/S0009250916303268
46. Sun, D., Tao, W.: A coupled volume-of-fluid and level set (voset) method for computing incompressible two-phase flows. International Journal of Heat and Mass Transfer **53**, 645–655 (1 2010). https://doi.org/10.1016/j.ijheatmasstransfer.2009.10.030, https://linkinghub.elsevier.com/retrieve/pii/S0017931009005717
47. Sussman, M., Puckett, E.G.: A coupled level set and volume-of-fluid method for computing 3d and axisymmetric incompressible two-phase flows. Journal of Computational Physics **162**, 301–337 (8 2000). https://doi.org/10.1006/jcph.2000.6537, https://linkinghub.elsevier.com/retrieve/pii/S0021999100965379

ICCS Camera Ready Version 2025
To cite this paper please use the final published version:
DOI: 10.1007/978-3-031-97570-7_29

48. Sussman, M., Smereka, P., Osher, S.: A level set approach for computing solutions to incompressible two-phase flow. Journal of Computational Physics **114**, 146–159 (9 1994). https://doi.org/10.1006/jcph.1994.1155, https://linkinghub.elsevier.com/retrieve/pii/S0021999184711557
49. Sussman, M., Smereka, P., Osher, S.: A level set approach for computing solutions to incompressible two-phase flow. Journal of Computational Physics **114**, 146–159 (9 1994). https://doi.org/10.1006/jcph.1994.1155, https://linkinghub.elsevier.com/retrieve/pii/S0021999184711557
50. Sweby, P.K.: High resolution schemes using flux limiters for hyperbolic conservation laws. SIAM Journal on Numerical Analysis **21**, 995–1011 (10 1984). https://doi.org/10.1137/0721062, http://epubs.siam.org/doi/10.1137/0721062
51. Tryggvason, G., Bunner, B., Esmaeeli, A., Juric, D., Al-Rawahi, N., Tauber, W., Han, J., Nas, S., Jan, Y.J.: A front-tracking method for the computations of multiphase flow. Journal of Computational Physics **169**, 708–759 (5 2001). https://doi.org/10.1006/jcph.2001.6726, https://linkinghub.elsevier.com/retrieve/pii/S0021999101967269
52. Tryggvason, G., Scardovelli, R., Zaleski, S.: Direct numerical simulations of Gas-Liquid multiphase flows (2011). https://doi.org/10.1017/CBO9780511975264
53. Tryggvason, G., Scardovelli, R., Zaleski, S.: The volume-of-fluid method, pp. 95–132. Cambridge University Press (1 2001). https://doi.org/10.1017/CBO9780511975264.006, https://www.cambridge.org/core/product/identifier/CBO9780511975264A041/type/book_part
54. Tsui, Y.Y., Lin, S.W.: Three-dimensional modeling of fluid dynamics and heat transfer for two-fluid or phase change flows. International Journal of Heat and Mass Transfer **93**, 337–348 (2 2016). https://doi.org/10.1016/j.ijheatmasstransfer.2015.09.021, https://linkinghub.elsevier.com/retrieve/pii/S0017931015009643
55. Unverdi, S.O., Tryggvason, G.: A front-tracking method for viscous, incompressible, multi-fluid flows. Journal of Computational Physics **100**, 25–37 (5 1992). https://doi.org/10.1016/0021-9991(92)90307-K, https://linkinghub.elsevier.com/retrieve/pii/002199919290307K
56. der Vorst, H.A.V., Dekker, K.: Conjugate gradient type methods and preconditioning. Journal of Computational and Applied Mathematics **24**, 73–87 (11 1988). https://doi.org/10.1016/0377-0427(88)90344-5, https://linkinghub.elsevier.com/retrieve/pii/0377042788903445
57. Welch, S.W., Wilson, J.: A volume of fluid based method for fluid flows with phase change. Journal of Computational Physics **160**, 662–682 (5 2000). https://doi.org/10.1006/jcph.2000.6481, https://linkinghub.elsevier.com/retrieve/pii/S0021999100964817

ICCS Camera Ready Version 2025
To cite this paper please use the final published version:
DOI: 10.1007/978-3-031-97570-7_29